INTERNATIONAL JOURNAL FOR NUMERICAL METHODS IN FLUIDS
Int. J. Numer. Meth. Fluids 2004; **44**:1299–1315 (DOI: 10.1002/fld.631)

Computations of two passing-by high-speed trains by a relaxation overset-grid algorithm

Jenn-Long Liu*,†,‡

Department of Information Management, Leader University No. 188, Section 5, An-Chung Road, Tainan 709, Taiwan, R.O.C.

SUMMARY

This paper presents a relaxation algorithm, which is based on the overset grid technology, an unsteady three-dimensional Navier–Stokes flow solver, and an inner- and outer-relaxation method, for simulation of the unsteady flows of moving high-speed trains. The flow solutions on the overlapped grids can be accurately updated by introducing a grid tracking technique and the inner- and outer-relaxation method. To evaluate the capability and solution accuracy of the present algorithm, the computational static pressure distribution of a single stationary TGV high-speed train inside a long tunnel is investigated numerically, and is compared with the experimental data from low-speed wind tunnel test. Further, the unsteady flows of two TGV high-speed trains passing by each other inside a long tunnel and at the tunnel entrance are simulated. A series of time histories of pressure distributions and aerodynamic loads acting on the train and tunnel surfaces are depicted for detailed discussions. Copyright © 2004 John Wiley & Sons, Ltd.

KEY WORDS: overset-grid technology; TGV high-speed train; inner- and outer-relaxation

1. INTRODUCTION

The high-speed rail system in Taiwan is being built to meet the requirements for rapid and mass transportation. The design speed of the Taiwan high-speed train (HST) is up to 350 km/h. For HST, the complicated flow in the aerodynamic and acoustic problems should be considered in advance. Particularly, as two trains pass by each other in a long tunnel or a train enters a tunnel, the complex fluctuations of aerodynamic loads and noise levels may cause concerns about operational safety, passengers' comfort and environmental issues. Previous work shows that when two trains moving in the opposite directions inside a tunnel,

*Correspondence to: Jenn-Long Liu, Department of Information Management, Leader University, No. 188, Section 5, An-Chung Road, Tainan 709, Taiwan, R.O.C.
†E-mail: linglong@ms23.hinet.net
‡Associate Professor.

Contract/grant sponsor: Ministry of Transportation and Communication; contract/grant number: MOTC-85-CSIST-08

Received 28 January 2003
Revised 31 July 2003

complicated transient pressure loads could act on the train bodies and tunnel wall [1–6]. In our design criterion, we would like to minimize the pressure rise. For example, a maximal pressure rise less than 8 kPa inside a tunnel is suggested to meet our design objective when one or two trains move in the tunnel. This value is proposed from consideration of the physiological limit that a human's ear membrane can bear. In general, adopting a streamlined HST body can decrease the pressure rise and drag force when a train moves in a tunnel. Also, using an adequate tunnel area not only can control the budget for construction cost, but also minimize the pressure rise when two trains pass by each other. Thus, to design a train body with aerodynamic shape and analyse a suitable cross section of the tunnel are very important in the HST construction. Another important topic is related to a moving train from the open field to a tunnel entrance. In this case, pressure waves are generated beforehand around the entry by the train. Owing to the superposition of non-linear waves with various wave speeds and amplitudes, a variety of weak pressure waves superimpose to form a high gradient compression wave that propagates toward the tunnel exit with the speed of sound plus the wave speed. When the plane compression wave reaches the exit, it partially radiates to the open field and also induces an expansion wave backward toward the entrance [7–9]. This unsteady flow simulation had been studied by the present algorithm and published in our HST's project report. For the sake of space limit, the results of this case are not presented here. We specifically propose a case that causes more concerns during our HST design phase. This case occurs when a train moves from the open field toward a tunnel entry, and passes by at the tunnel entrance with another train moving inside the tunnel toward the open field. Finally, the two trains pass each other at the tunnel entrance. For this case, it is worthwhile to analyse the flow field in order to further clarify the amplification of aerodynamic loads.

As we know, when two trains pass by each other in the opposite directions, it is an inherently unsteady flow and the experiment for a scale-down model or prototype test is difficult. We not only need to construct a long track, but also need to use a dynamical data acquisition system for data measurement. Thus, for studying the dynamical problem of moving trains, the use of a numerical approach seems to be a good way for studying design options. In recent years, many numerical methods have been presented and applied to a large variety of complicated engineering problems. However, if the geometries of the problems analysed are more complex, it is more difficult to deal with the grid generation by using numerical approaches. Generally speaking, using a single mesh for a complex configuration or multi-geometry is workable, but the computation will become inefficient and the solution may be inaccurate, especially for high Reynolds number flows. In addition, if the domain of interest has a relative motion between configurations, regeneration of the grid would be required in each time step. Obviously, when a single-grid methodology is applied for three-dimensional computations of a moving body, the reconstruction of grids throughout the entire domain could be quite troublesome, inefficient and expensive. On the other hand, multi-grid technique applied to the computation including multi-body or complex geometry is more feasible than the single-mesh method. It can yield a better grid resolution, simplify the boundary conditions, and alleviate the task of grid regeneration. As we know, two types of multi-grid methods are the patched and overset methodologies. For the patched grid method, boundary surfaces of one mesh are connected with adjacent surfaces of other mesh. For the overset grid method, multiple meshes are generated independently for each configuration or domain of interest, and are then superimposed to form a global mesh system. Although the patched grid method can be used

to deal with complex geometry problems, it is hard to handle problems in which the bodies or configurations have relative motion. The overset minor meshes are independent of each other in the global mesh system, and they can move independently with respect to other grids [10, 11]. Therefore, this method provides a more powerful strategy for solving unsteady problems. The bookkeeping technique is fully capable of tracking the overset relationship between the moving mesh and stationary grids. Successful calculations using numerical methods have been reported in the References [11, 12]. In this paper, we use the overset method for the unsteady flows of moving high-speed trains and also propose a time relaxation method by inner and outer iterations to improve the accuracy of the unsteady solution. The relaxation process is desired for highly unsteady flow simulation, especially for the case of two high-speed trains passing by each other in a tunnel or passing by each other at a tunnel entrance.

2. NUMERICAL ALGORITHM

A three-dimensional program named HYDRA [13], based on the overset grid technique [10] and a finite difference flow solver [14], is used. The program is further developed in the present computational work to achieve the efficiency and correctness in hole bookkeeping, interpolation treatment and viscous terms. To calculate the highly unsteady HST flow, an accurate time relaxation method using inner- and outer-relaxation process is also included in the program package.

2.1. Navier–Stokes flow solver

Several researchers have used the Euler equations to simulate the HST flow [3, 7], though it is well known that these solutions will differ from the true viscous flow. In general, when applying inviscid flow solvers to the HST flow, the rear nose of the train must be sharpened to avoid creating an unreasonable wake flow. For the computation of two trains passing each other, since the wake effect cannot be captured by the inviscid code, the interaction effect of the wake flows on the trains is lost. On the other hand, using a viscous flow solver allows these effects to be simulated and results in a reliable solution. The governing equations for the HST flow used here are the unsteady, compressible, thin-layer, Navier–Stokes equations. The Reynolds number is specified as 6.7×10^6, which is based on air properties at the ground surface, train speed and maximum width of the train. As we know, in the high Reynolds number limit, viscous effects are concentrated near rigid boundaries and in wake regions. Typically in computations we only have enough grid points available to concentrate grid lines near the rigid surfaces. Even though we may program the full Navier–Stokes equations, the viscous terms associated with derivatives along the body will not be resolved and in cases for attached and mildly separated flows these terms are negligible. The terms in the near normal will be resolved for sufficiently fine grid spacing and these are substantial terms. In the present study it is also assumed that a front skirt is not installed at the train nose and there is no cross wind. In this case, separated flow is observed from oil flow studies to occur at the rear of the train. Thus, the thin-layer Navier–Stokes flow solver combined with two-layer algebraic turbulent model is adequate to simulate the HST flow field. Applying the thin-layer approximation, all the viscous terms associated with ξ and η derivatives are neglected. The

equations can be rewritten in non-dimensional form in the generalized curvilinear co-ordinates as follows [14]:

$$\frac{\partial Q}{\partial t}+\frac{\partial E}{\partial \xi}+\frac{\partial F}{\partial \eta}+\frac{\partial G}{\partial \varsigma}=R_e^{-1}\frac{\partial S}{\partial \varsigma} \tag{1}$$

The turbulent effect is accounted for by using the Baldwin–Lomax model and was designed specially for use with the thin-layer approximation [15]. Using a central difference scheme and an implicit approximate factorization for Equation (1), the non-linear governing equations can be formulated as

$$\begin{aligned}&(I+h\delta_\xi A^n)(I+h\delta_\eta B^n)(I+h\delta_\varsigma C^n-hR_e^{-1}\delta_\varsigma J^{-1}M^n)\Delta Q^n\\&\quad=-h(\delta_\xi E^n+\delta_\eta F^n+\delta_\varsigma G^n-R_e^{-1}\delta_\varsigma S^n)\end{aligned} \tag{2}$$

Here, $\Delta Q^n=Q^{n+1}-Q^n$ and $h=\Delta\tau$. The three-dimensional flux Jacobian matrices A^n, B^n, C^n and M^n are presented in Reference [14], and their expressions are not listed here. The spatial derivative operators δ_ξ, δ_η and δ_ς are approximated by second-order central difference. In addition, the second- and fourth-order artificial dissipation terms with non-linear coefficients are added in the left- and right-hand sides, respectively, for numerical stability [14].

2.2. Time relaxation method

In the current work, we propose a relaxation method to achieve a time-accurate solution for unsteady flow. The relaxation method can easily be included into the approximated factorization scheme to iterate the flow properties. First, we replace the Jacobian matrices A^n, B^n, C^n and A^n, B^n, C^n and M^n with $A^{(m)}, B^{(m)}, C^{(m)}$ and $M^{(m)}$, respectively, for computing temporary, intermediate values. Second, we include an inner- and outer-relaxation process for the time-marching iteration. Since the flux terms on the right-hand side of Equation (2) do not change, the time level accuracy is maintained in the current time step. One cycle inner iteration is completed by implementing two iterations $m=1$ and 2. When the index m equals to one, numerical computation is performed from the point $(i,j,k)=(2,2,2)$ to the point $(i\max-1, j\max-1, k\max-1)$. Here, the symbols $i\max$, $j\max$ and $k\max$ are defined as the maximum grid numbers in the x, y and z directions, respectively. The reverse sweep direction is performed from $(i\max-1, j\max-1, k\max-1)$ to (2, 2, 2) when the index m equals to two. Therefore, Equation (2) can be rewritten in the following form:

$$\begin{aligned}&(I+h\delta_\xi A^{(m)})(I+h\delta_\eta B^{(m)})(I+h\delta_\varsigma C^{(m)}-hR_e^{-1}\delta_\varsigma J^{-1}M^{(m)})\Delta Q^{(m)}\\&\quad=-h(\delta_\xi E^n+\delta_\eta F^n+\delta_\varsigma G^n-R_e^{-1}\delta_\varsigma S^n)\end{aligned} \tag{3}$$

$$Q^{(m+1)}=Q^{(m)}+\omega_n\Delta Q^{(m)},\quad m=1,2 \tag{4}$$

For steady-state flow, only one cycle $(m=1,2)$ for inner iteration is used in the time level n. For unsteady flow calculation, several cycles are required until the variable $\Delta Q^{(m)}$ reaches a quasi-steady state. In the present calculation, the quasi-steady state is reached when the root

mean square of residual term $\Delta Q^{(m)}$ less than 10^{-5}. At the end of inner relaxation, an outer relaxation process is introduced as follows:

$$Q^{n+1} = Q^n + \omega_{\text{out}} \Delta Q^{(m)} \tag{5}$$

In Equations (4) and (5), the coefficients ω_{in} and ω_{out} are defined as inner and outer relaxation parameters, respectively. The inner relaxation parameter ω_{in} can take as over-relaxation for achieving fast convergence. In this paper, the value of ω_{in} is specified as 1.2. In general, the quasi-steady state is easily obtained after 3–5 inner iterations. It is noted that the value of ω_{out} should be chosen as 1.0 for unsteady flow computation. From our study, the relaxation method will achieve time-accurate solution.

2.3. Iteration procedure on the Navier–Stokes flow solver and multi-block overset grid scheme

The multi-block overset grid scheme is capable of tracking the bookkeeping of multiple meshes, boundary points and hole points. The hole points that result from the grid points of one mesh and fall within another body boundary must be blanked or excluded from the solution calculation [10]. This process is easily established. First, we define an array variable IBLANK to record hole information for all grids, and then multiply the implicit and explicit matrices shown in Equation (3) by the array variable. The array variable is defined as

$$\text{IBLANK} = \begin{cases} 1 & \text{if a point is not blanked} \\ 0 & \text{if a point is blanked} \end{cases} \tag{6}$$

For example, if points p and q are two hole points, then the two points are excluded from the computation. It means that the values for ΔQ_p^n and ΔQ_q^n are not changed. Besides, if the outer boundary points of one minor mesh located within another minor or major mesh, the flow solution is updated by the interpolation routine from the solutions of minor or major mesh. In the present HST computation, since the bottom of the train body is very close to the ground surface, an effort is made to distribute the grid in this region. If the remaining grid points in the region between the train bottom and ground surface are not enough after hole grids are blanked from the tunnel mesh, the viscous effect cannot be simulated correctly. To resolve this problem, we generate finer grids in the tunnel mesh near the ground surface to achieve accurate viscous simulation. The grid topology used here is O–O-type mesh for the train body, and O–H-type mesh for the tunnel/open field. The fine grid distribution is generated around the train surface. The minimum distance between the adjacent point and train body is near 1.0×10^{-5}, and it is small enough to resolve the boundary layer flow. In the two trains passing-by case, about 42 0000 grid points are generated for the train and tunnel within the computational domain. These types of grid distribution can provide better numerical solution through our computational study.

2.4. Boundary conditions

In this paper, the boundary conditions on the train body, tunnel wall, tunnel entrance and ground surface should be established in the computational domain. First, the contravariant velocities are set to be zero both on the stationary tunnel wall and ground surface. The pressure and density on the surfaces are simply set as the values from adjacent field points.

For the moving HST body, the grid speeds on the train mesh are all specified as the train speed. In addition, the pressure is obtained by computing the momentum equations [14].

At the tunnel entrance, exit and open field, characteristic boundary conditions are applied. The incoming Riemann invariant is specified as freestream condition, and the outgoing invariant is extrapolated from interior points. Using the invariants, we can figure out the normal component of velocity and speed of sound [14]. When two trains pass in a tunnel, the tunnel is assumed long enough, so the boundary conditions on the right and left ends of computational domain are using the characteristic boundary conditions. For the case of a train moving out from a tunnel and another train moving toward the tunnel, the flow properties at the tunnel end are easily implemented by using the overlap grid technology. Except for the single stationary HST computation, only one-half of the flow field is computed to reduce the large amount of CPU time. Thus, additional boundary conditions on the symmetric tunnel centreline should be established. It is easily implemented by using point symmetry condition. Under this condition, the u, v and w are set as anti-symmetric about the symmetrical centreline.

3. RESULTS AND DISCUSSIONS

3.1. Flow passing through a stationary TGV high-speed train in a long tunnel

To evaluate the numerical accuracy of the present algorithm for the HST problem, a wind tunnel test for a stationary train located in a long tunnel was conducted. In this case, the train model was chosen as French high-speed TGV, and the cross-sectional area of tunnel was specified as $90\,\mathrm{m}^2$. In addition, the flow speed was specified as 350 km/h which corresponds to a Mach number of 0.28. In the experiment, we measured static pressures along the train's upper centreline and side surface for the numerical evaluation purpose, and the pressure distributions are displayed in Figure 1. From Figure 1(a), it is clearly seen that the stagnation point is located at the train nose. It is evidently demonstrated that the pressure drops significantly after the train nose, and then increases near the wedge-like windshield. As flow pass over the windshield, it produces a strong flow expansion such that the pressure decreases rapidly. From the figure, the comparison between computational and experimental results is in good agreement. Figure 1(b) shows the comparison of pressure distribution along the train's side surface. Since the locations of experimental pressure holes and numerical grid points are not exactly identical, there exist little discrepancies in this pressure comparison. However, the trend is well predicted. On the tunnel wall, Figures 2(a) and 2(b) display the pressure distributions along the tunnel's upper centreline and side surface. It is clearly depicted that the evaluation by the presented numerical algorithm is quite good. In this paper, the flow solver has been verified through many test cases to evaluate the numerical accuracy of viscous flow. In the experimental HST flow, our wind tunnel test is carried out only for pressure data measurement, so no comparison of skin friction distribution with the numerical computation can be presented in the paper. In the HST design process, we are more concerned with the aerodynamic loading.

3.2. Two TGV high-speed trains passing by each other in a long tunnel

The schema of two TGV high-speed trains passing by each other in a long tunnel is demonstrated in Figure 3. The two trains are moving in the opposite directions. It is mentioned

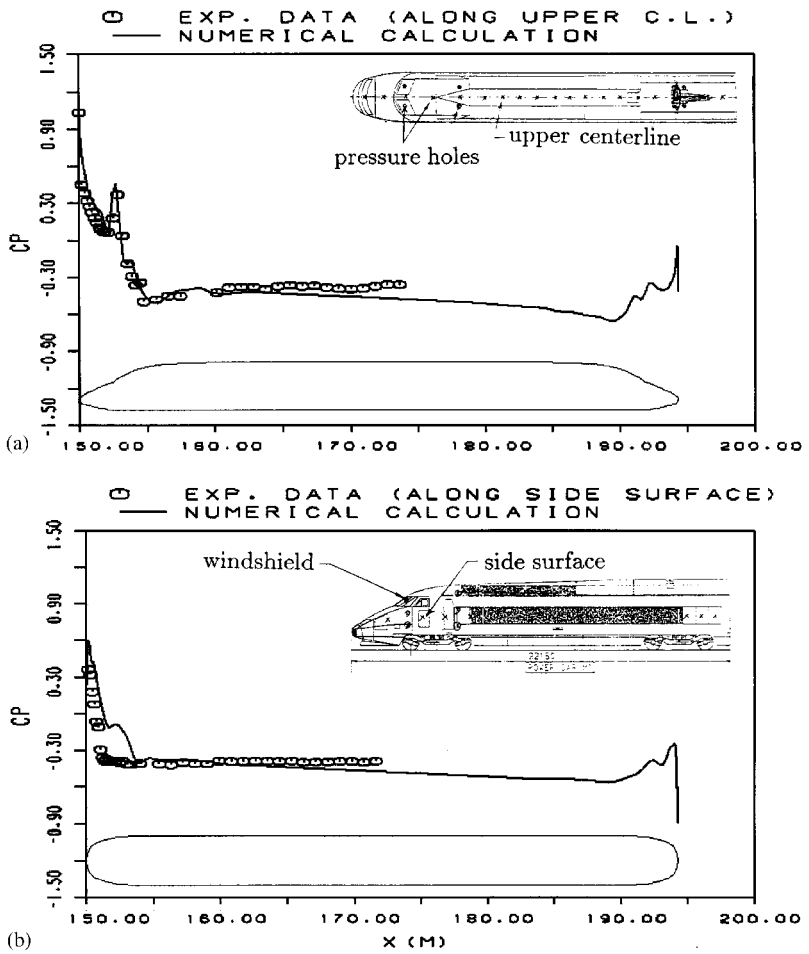

Figure 1. Pressure distributions along the (a) upper centreline and (b) side surface on the train body for flow passing through a single stationary TGV train.

above that the distance between the train body and ground surface is relatively small, and it is required to generate finer grids in this region for the viscous solution. For analysing the sequential variations of pressure and aerodynamic load, we chose six locations labelled by the symbols A, B, C, D, D′ and E for recording data. The symbols A and B indicate the positions on the front and rear train noses, respectively. Point C indicates the windshield position, and points D and D′ are set as the positions at both side doors of train. Point E represents the symmetric centre on the upper tunnel wall. In the present study, the cross-sectional area of tunnel is chosen as $90\,m^2$, and two TGV trains are moving with a high speed at 350 km/h in the opposite directions. Also, the tunnel length is assumed to be long enough such that the pressure waves generated by the train entry can be neglected.

Using the present algorithm, the time histories of pressure contours on the train body and ground surface are displayed in Plate 1. As shown in Plate 1, when the two trains approach

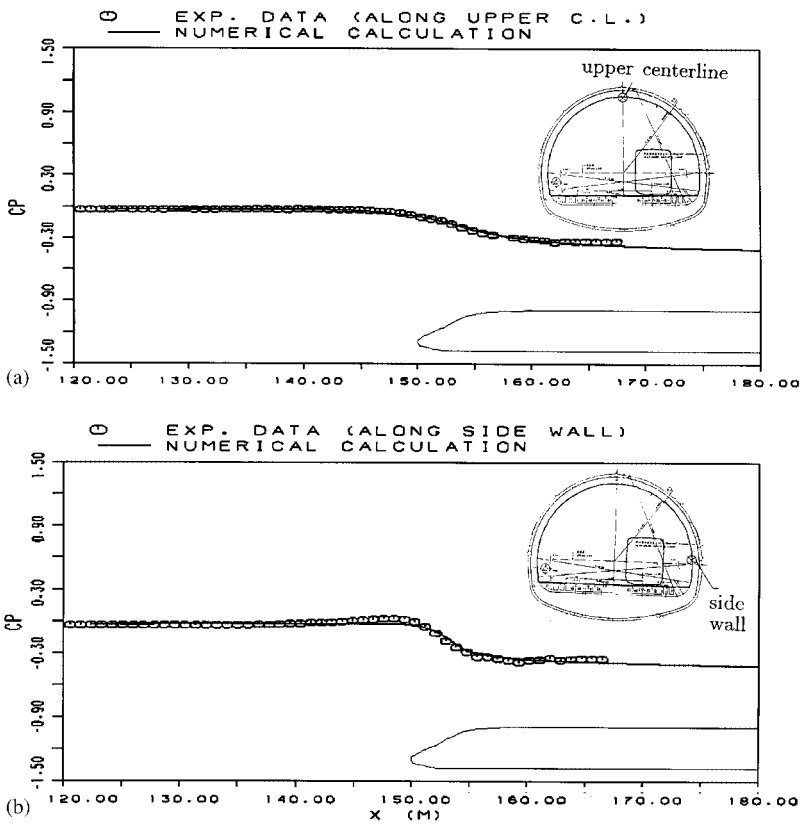

Figure 2. Pressure distributions along the (a) upper centreline and (b) side wall on the tunnel surface for flow passing through a single stationary TGV train.

each other, fluid between the two train noses are compressed. Thus, the pressure increases quite rapidly when the distance dx is from 33.31 m to 16.51 m. The symbol dx used here represents the distance between the two train noses. A positive dx indicates that the two train noses have not passed each other yet, while a negative value means contrarily. In addition, in the pressure contour plots, white and red colors represent high pressure-levels, while green and blue colors represent low levels. In Plate 1(a), the pressure on the front nose reaches a maximum when dx equals 10.89 m. As soon as the train noses pass by each other, the pressures on the front nose and windshield decrease. At that time, the compression waves created from the compression by the two trains before passing by each other will move toward downstream. When dx equals -5.91 m, the compression waves just pass through both rear train noses. As the two trains moved further in the range of dx from -11.52 to -45.14 m, the blockage ratio becomes large such that a significant flow acceleration is produced and a rapid pressure decrease results. In this calculation, the minimal pressures on both rear noses occur when dx equals -84.36 m. In this paper, we use the 'blockage ratio' to describe the area occupied by one or two trains in a tunnel. The definition of blockage ratio is the ratio of maximum cross-sectional area of the trains to the tunnel area (90 m^2). As the two trains

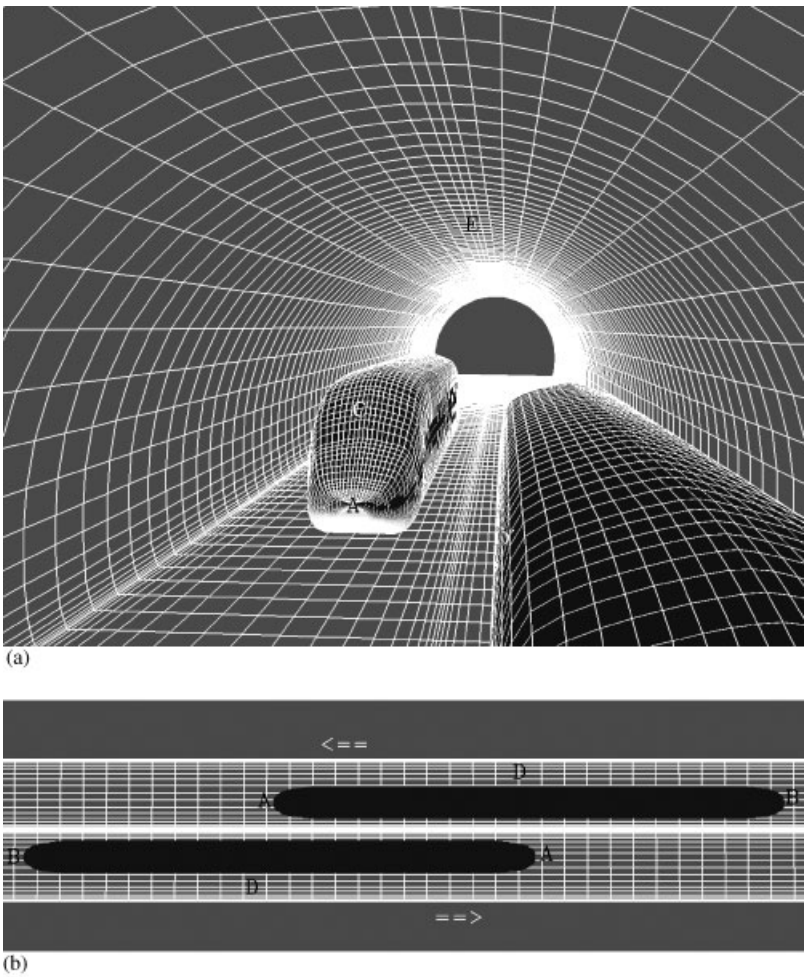

Figure 3. The illustrations of (a) front and (b) top views for the two TGV trains passing by each other in a long tunnel.

move away from each other, the pressures on the front noses recover to the same level as that of a single train moving in the long tunnel.

To further analyse the variations of pressure and aerodynamic loads, time histories of pressure at the six recording points are presented. The pressures at the points A–E are plotted in Figure 4. From Figure 4(a), it is observed that the pressures at the points A and C increase to maximum levels when the distance dx is about 11 m. At this time, the pressures on the front nose and windshield are evaluated as 15.4 and 13 kPa, respectively. As soon as the two front noses pass each other, the pressures on the nose and windshield decrease rapidly to relatively low values until the two trains are nearly side by side. Afterwards, the pressures at points A and C recover gradually to 6.5 and 4.75 kPa. At the rear nose (point B), the pressure first maintains a low value and gradually increases to 2.54 kPa when dx is near to

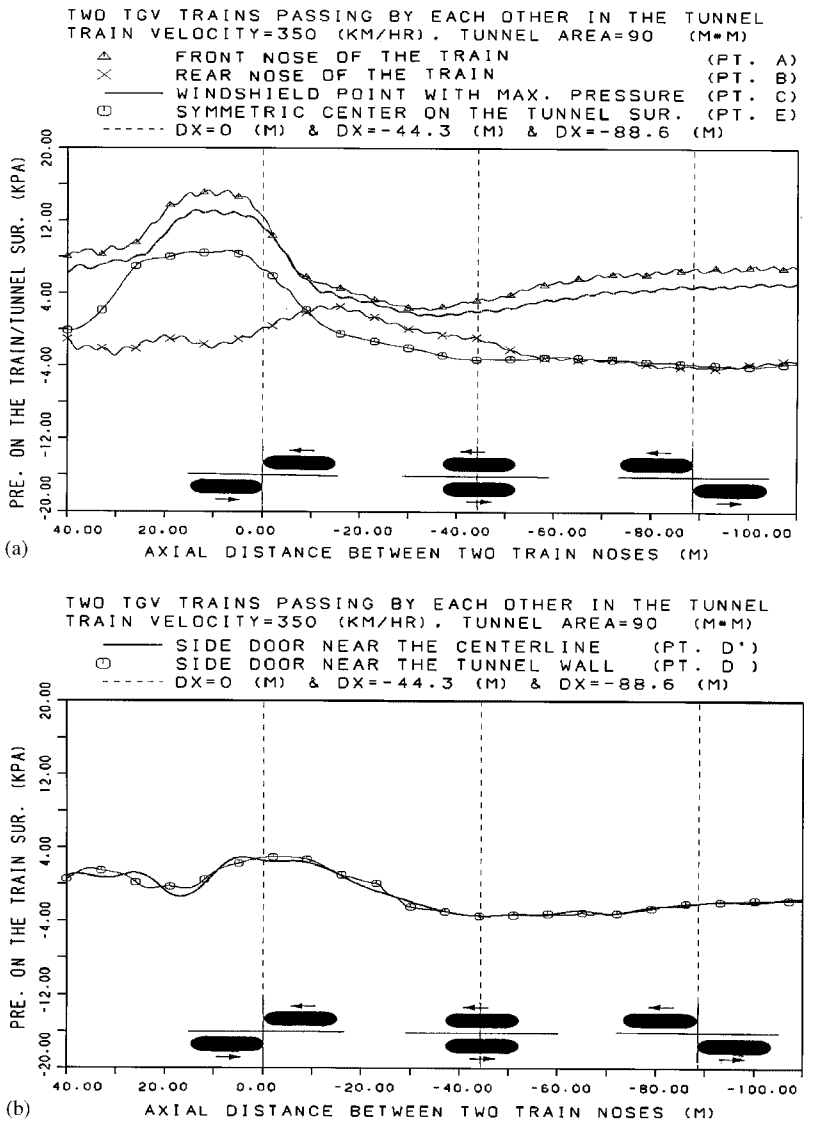

Figure 4. Time histories of pressure distribution on the points (a) A, B, C, E and (b) D and D′ for the two TGV trains passing by each other in a long tunnel.

−15.7 m. Finally, when the two trains passed, the pressure at the point B drops to −4.0(kPa). At the point E, the pressure increases rapidly as the trains approach each other, and then decreases gradually due to flow acceleration after the two train noses pass by each other. The pressures on the side doors (at points D and D′) are plotted in Figure 4(b). From the figure, the pressure changes are not remarkable.

To verify the present numerical solution, we cite an analytical datum reported by the French Sofrerail Corp. and also use an empirical solution for the comparison. As shown in the

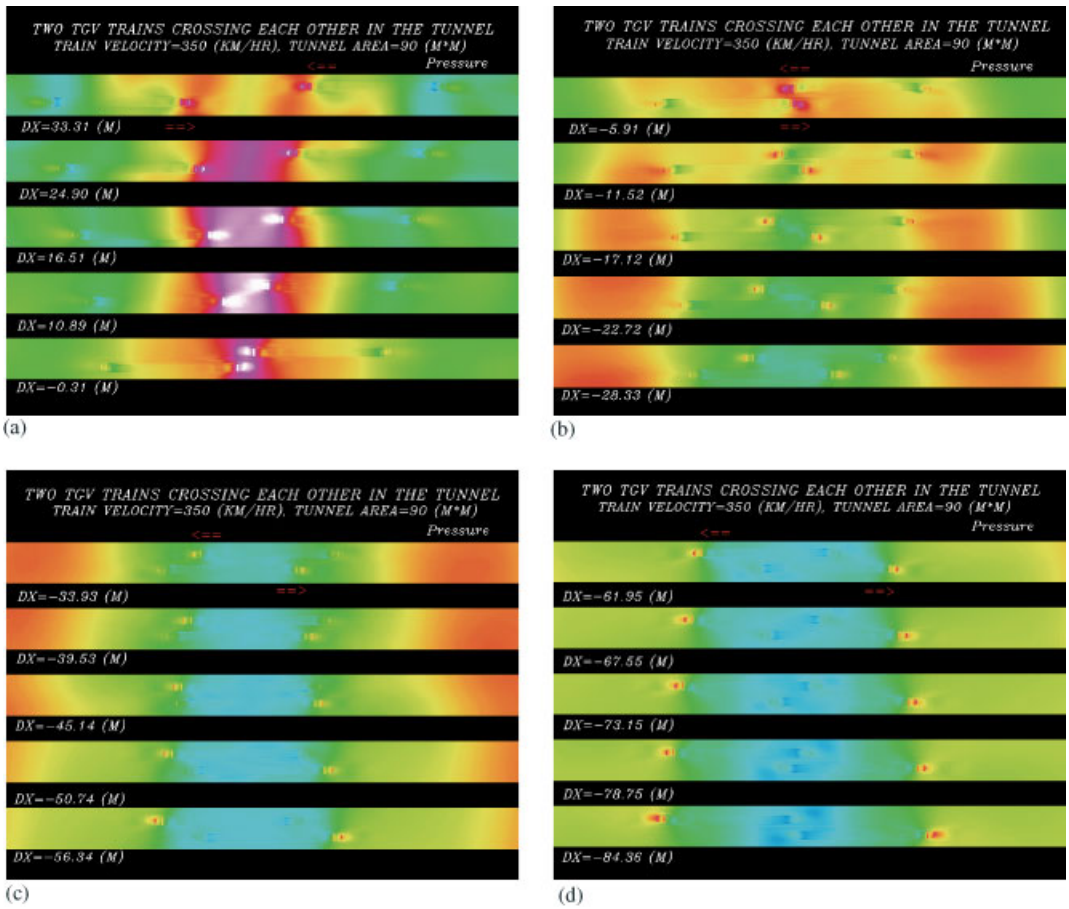

Plate 1. Top views of pressure contours for the two TGV trains passing by each other in a long tunnel.

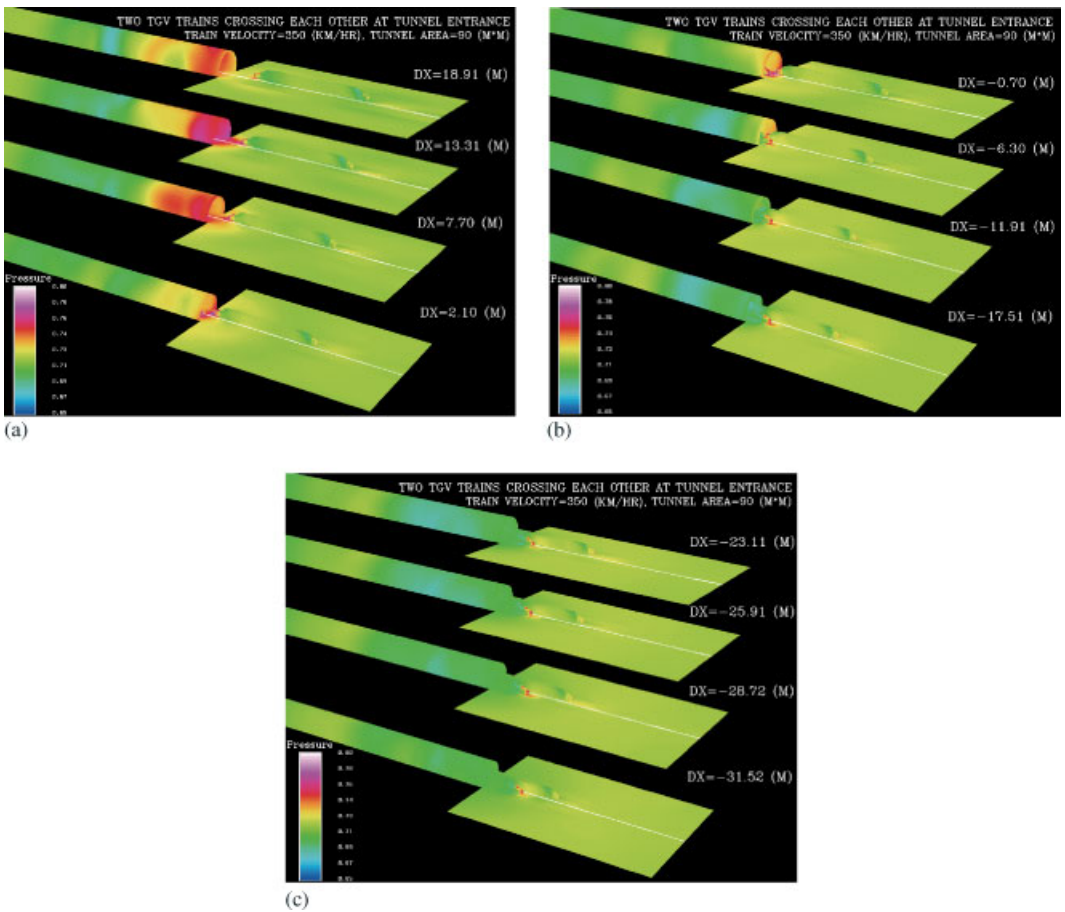

Plate 2. Side views of pressure contours for the two TGV trains passing by each other at the tunnel entrance.

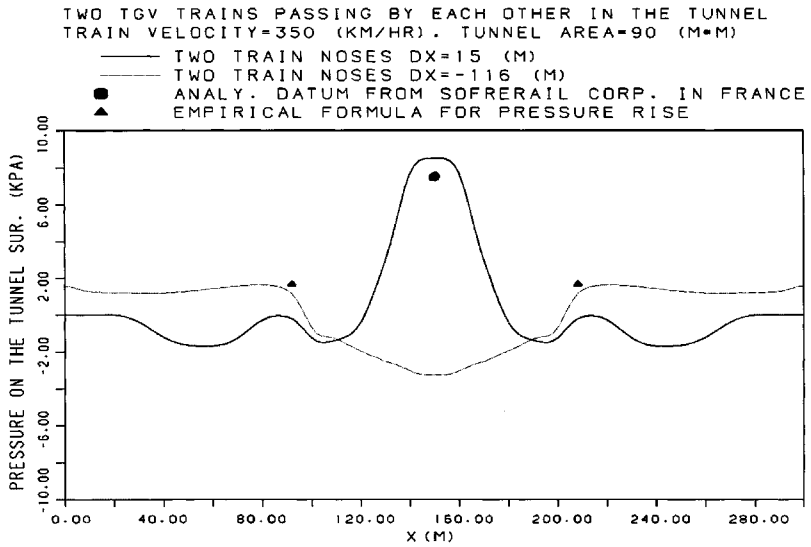

Figure 5. Comparison of pressure rises of the present calculation with the Sofrerail's datum and empirical formula.

Figure 5, the maximal pressure rise in the present calculation is 9 kPa, and Sofrerail's datum is 8 kPa. The higher value obtained by the present approach is quite reasonable for our non-linear viscous calculation. Further, when the two trains move away from each other, the pressure on the tunnel wall by the present approach is close to the empirical solution about 1.68 kPa. Also, the comparison is quite agreeable.

Besides, the aerodynamic loads acting on the train should also be investigated since it directly influence the passengers' comfort and HST's operational safety. Figure 6 shows the time histories of aerodynamic force and moment on the train. When the two trains approach each other, the drag force first increases, then decreases due to the pressures drop at the front noses, and then increases gradually after the nose stagnation pressure recovers. For the side force C_Y, it also increases when the trains approach each other. The positive C_Y indicated here means that the side force tends to push the trains apart from each other. As the two trains are side by side, the side force decreases to a minimum. In the present calculation, the position of maximum side force is located at about dx equal to -7 m. This datum is reasonable when compared with the value -6.5 m displayed in Reference [2], which simulated two SKS-like trains passing by each other inside a tunnel with a train speed of 270 km/h. When dx equals to -45 m, the side force decreases to a negative value. This implies that the side force tends to pull the trains close to each other. After the trains move away from each other, the side force C_Y becomes relatively small. The variation of lift coefficient C_L is small in the period during which two trains pass by each other. The histories of the aerodynamic moments are plotted in Figure 6(b). In this figure, it is obviously that the effect for yawing moment is the main consideration in the HST's design. The variation of C_N has a similar trend as that of the side force C_Y. As the two trains approach each other, the positive C_N will turn the trains apart from each other and the negative value will turn them back together after the trains are in the side by side position. The variations of rolling moment and pitching moment in the

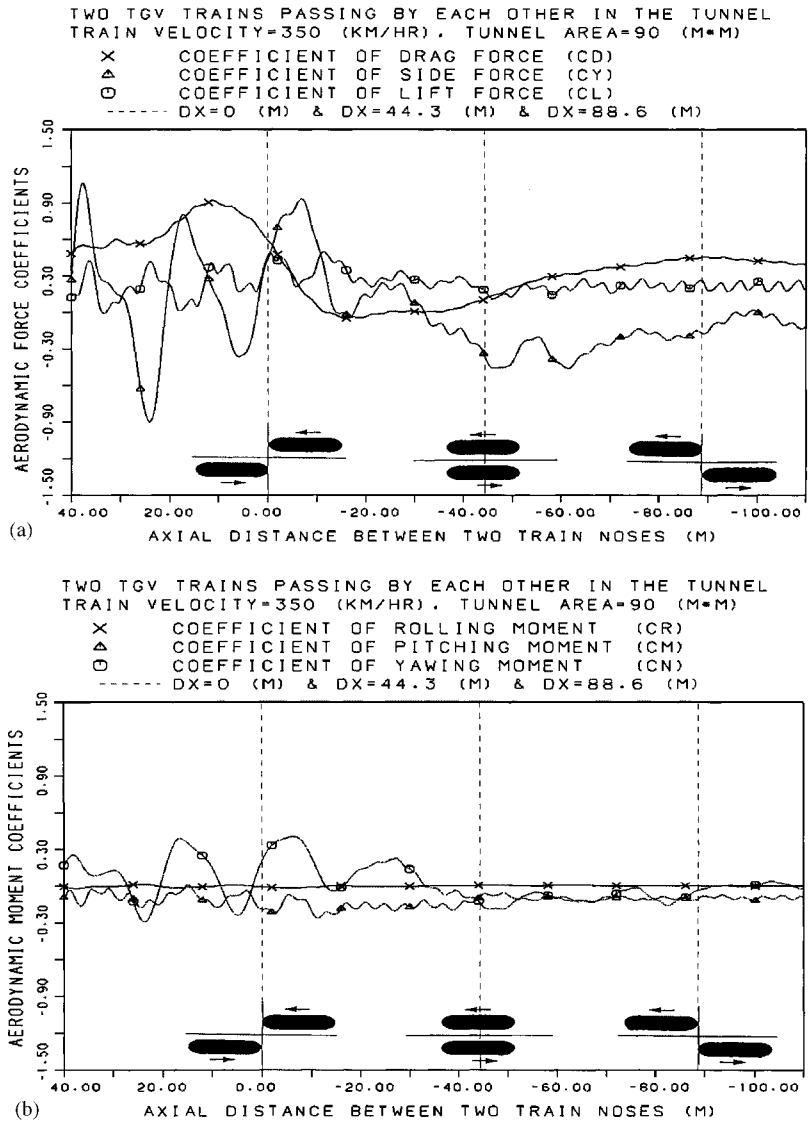

Figure 6. Time histories of the (a) aerodynamic forces and (b) moments on the train body for the two TGV trains passing by each other in a long tunnel.

present calculation are quite small. This implies that the TGV train has a good quality for the passengers' comfort and the train's stability. In this case, long distance is set between the two trains before passing by. Thus, it requires a large amount of CPU time to compute the unsteady HST flow. For this case, about 300–400 h of CPU time were used for the simulation on an HP 750 workstation.

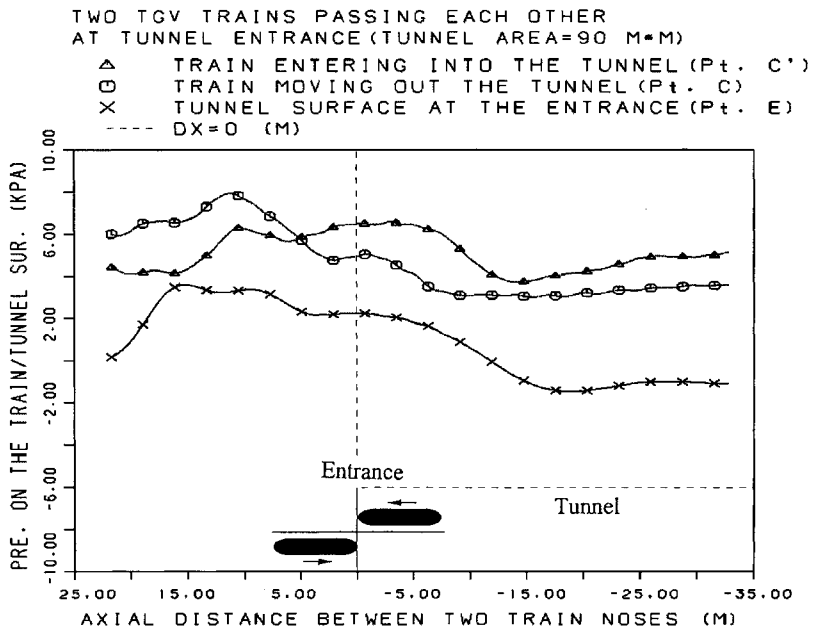

Figure 7. Time histories of pressure distributions at the points C, C′ and E for the two TGV trains passing by each other at the tunnel entrance.

3.3. Two TGV trains passing by each other at the tunnel entrance

In the design consideration for two high-speed trains passing by each other, we usually study the case that two trains pass by each other in the open field or pass by each other inside a tunnel. However, the case that two trains pass by each other at a tunnel entrance should also be included in the design consideration. For this case, the blockage ratio is larger than that for the case of only one train entering a tunnel and it also has the effect of two trains passing each other. Thus, to complete the aerodynamic analysis before the construction of HST, a detailed analysis for this case is necessary. In this paper, we simulate the flow field of two trains passing by each other near a tunnel entrance. Plate 2 shows the pressure contours for various distances of dx. For the sake of explanation, we define the train-I as the train moving out of the tunnel and the train-II as the train entering the tunnel.

In this case, when the distances between the front noses of the two trains is in the range of 18.91–13.31 m (as shown in Plate 2(a)), the pressures at the two noses and at the tunnel entrance increase rapidly. As the distance decreases to 7.7 m, the high compression waves generated by the train-I partially radiate outward to the open field and propagate along the semi-spherical direction. After the train-I passes by the train-II at the portal, a large blockage effect causes the pressures on the tunnel surfaces decrease rapidly (as shown in Plate 2(b)), $dx = -0.7\,\text{m} \sim -17.51\,\text{m}$. It is noted that the high-gradient plain compression wave has not clearly formed for this case because of the train-I moving out from the tunnel such that the waves generated by the train-II does not have enough evolution space to consolidate wave strength. In general, steep compression waves are formed in the case of train entry [7–9]. As dx changes from -23.1 to -31.52 m, as shown in Plate 2(c), the nose of train-I moves

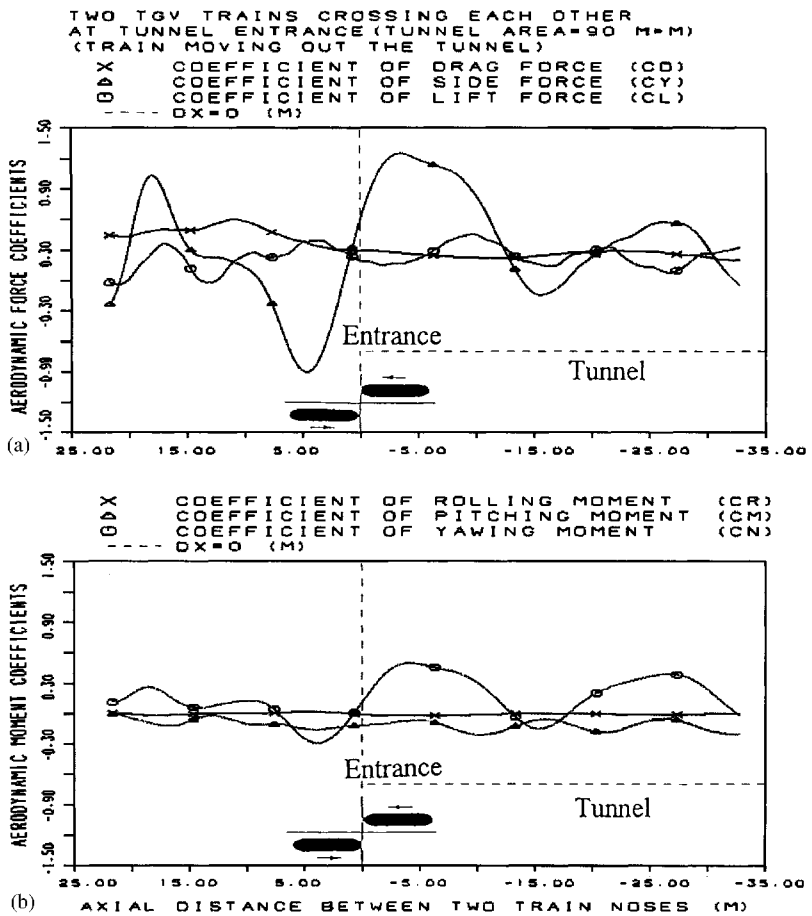

Figure 8. Time histories of the (a) aeordynamic forces and (b) moments on the train-I's body for the two TGV trains passing by each other at the tunnel entrance.

out further to the open field, such that the pressure on the windshield decreases. It is also displayed in Plate 2(c) that the pressures are low except at the front nose and windshield.

Figure 7 shows the pressure distributions at the tunnel entrance (point E). The positions at the windshield of train-I and train-II are denoted as point C and C′. When dx equals to 11 m, a maximal pressure of about 7.9 kPa is observed at the train-I's windshield. It is also indicated that the maximum pressure at the tunnel entrance will increase to 3.6 kPa. Furthermore, as the train-I moves further toward the entrance, high pressure induced by train-I reaches the entrance. Meanwhile, expansion waves are generated and then propagate back to the tunnel and the micro-pressure waves radiate to the open field. Thus, the pressure at the nose of train-I decreases and of train-II increases. As the train-I moves out the tunnel from a confined domain to a large open field, the pressure on the windshield decreases to 3.5 kPa. On the other hand, the train-II moves from the open field into the confined tunnel, the pressure on the windshield first increases to 6.5 kPa, and then decreases to 3.73 kPa due to the influence

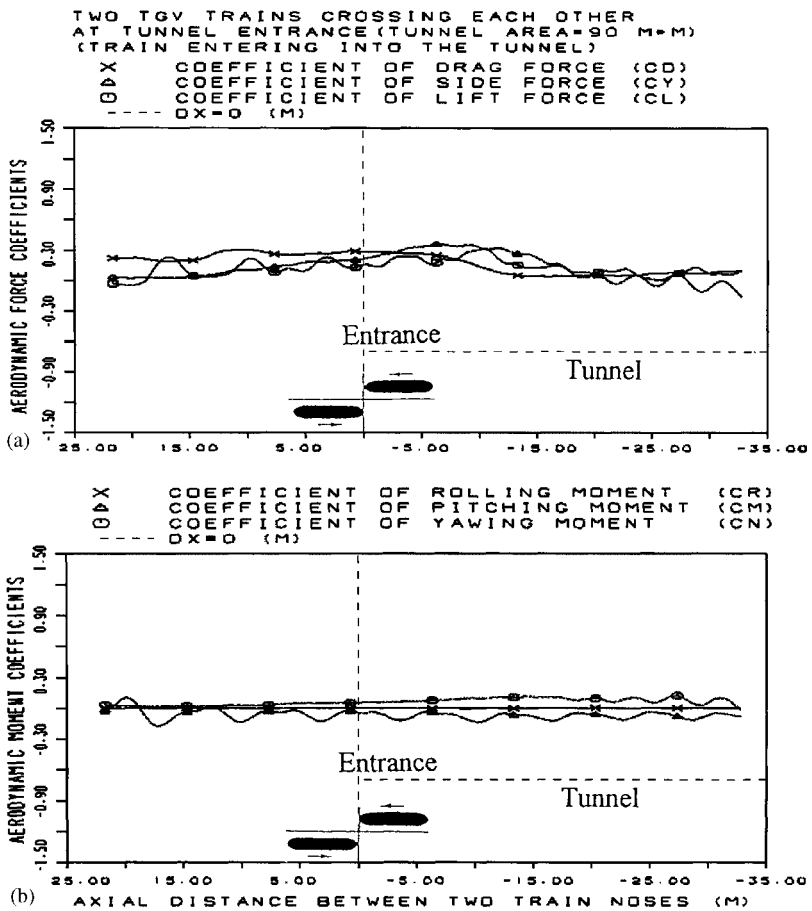

Figure 9. Time histories of the (a) aeordynamic forces and (b) moments on the train-II's body for the two TGV trains passing by each other at the tunnel entrance.

of low pressures spread out around the shoulder of train-I. At the tunnel entrance (at point E), the pressure decreases continuously from the maximum value of 3.6 to -1.49 kPa. The aerodynamic loads of the train-I and train-II are shown in the Figures 8 and 9,respectively. From Figure 8, the side force and yawing moment change considerably. The load variations of train-II as displayed in Figure 9 are obviously relatively small. Therefore, more concern should be given to the train-I for HST's operational safety and passengers' comfort during two trains passing by each other at a tunnel entrance. From Figures 8 and 9, the oscillations of aerodynamic loading resulted from the wave interaction can be seen. When the compression wave generated by train-I reaches the tunnel entrance, pressure waves radiate to the open field partially, and others reflect as expansion waves and propagate backward into the tunnel. On the other hand, the compression wave generated by train-II moves toward the tunnel. The two kinds of non-linear waves interact with each other and produce unsteady load fluctuations on the train bodies.

4. CONCLUSIONS

The overset grid methodology is used to resolve the difficulty in the grid generation for unsteady flows of moving high-speed trains. The three-dimensional unsteady, compressible, thin-layer, Navier–Stokes equations are solved by an approximate factorization method. To achieve the time-accurate solution, the inner- and outer-relaxation method is also included. The relaxation method is desired for computing inherently unsteady flow fields of high accuracy. In this paper, pressure measurements were presented for a single stationary TGV train inside a long tunnel by using the low-speed wind tunnel test. The experimental pressure distributions validate our numerical evaluations. It is shown that the comparison for the pressure distributions between the computation and experiment is good. Further, two cases are simulated for two trains passing by each other. One case is that two TGV trains pass by each other inside a long tunnel, and the other case is that the two TGV trains pass by each other at a tunnel entrance. From the numerical results, the pressure values and aerodynamic loads are strongly dependent on the relative positions of the trains. When the two trains approach each other, high pressure is generated at the train noses. In addition, strong side force and yawing moment variations are also induced and they are of concerns for the HST's operational safety and passengers' comfort. In the present calculation, the maximum pressure rise inside the tunnel is around 9 kPa at the conditions of train speed and tunnel cross-sectional area equal to 350 km/h and 90 m^2, respectively. This result implies that the shape of the train and cross-sectional area of the tunnel are adequate in the practical HST operation for a train speeds under 250 km/h. For the two trains passing by each other at a tunnel entrance, a complicated flow field results from the interaction of the trains. In this case, more concern should be given to the train that moves from the tunnel to the open field due to large variations in the side force and yawing moment.

ACKNOWLEDGEMENTS

The author is grateful for the support provided by the Bureau of High-Speed Rail of Ministry of Transportation and Communication under grant MOTC-85-CSIST-08.

REFERENCES

1. Ogawa T, Fujii K. Numerical simulation of compressible flow induced by a train moving in a tunnel. *AIAA Paper 93-2951*, 1993.
2. Fujii K, Ogawa T. Aerodynamics of high speed trains passing by each other. *Journal of Computers and Fluids* 1995; **24**:897–908.
3. Ramakrishnan SV, Chen CL, Chakravarthy SR, Szema KY. Numerical simulation of two opposing high-speed trains in a tunnel. *AIAA Paper 95-0746*, 1995.
4. Kikuchi K, Maeda T, Yanagizawa M. Numerical simulation of the phenomena due to the passing-by of two bodies using the unsteady boundary element method. *International Journal for Numerical Methods in Fluids* 1996; **23**:445–454.
5. Howe MS. Pressure transients generated when high-speed trains pass in a tunnel. *Journal of Applied Mathematics* (*SIAM*) 2000; **65**:315–334.
6. MacNeill RA, Holmes S, Lee HS. Measurement of the aerodynamic pressures produced by passing trains. *Proceedings of the 2002 ASME/IEEE Joint Rail Conference*, Washington, D.C., 2002.
7. Mestreau E, Löhner R, Aita S. TGV tunnel entry simulations using a finite element code with automatic remeshing. *AIAA Paper 93-0890*, 1993.
8. Howe MS, Iida M, Fukuda T, Maeda T. Theoretical and experimental investigation of the compression wave generated by a train entering a tunnel with a flared portal. *Journal of Fluid Mechanics* 2000; **425**:111–132.

9. Auvity B, Bellenoue M, Kageyama T. Experimental study of the unsteady aerodynamic field outside a tunnel during train entry. *Experiments in Fluids* 2001; **30**:221–228.
10. Steger JL, Benek JA. On the use of composite grid schemes in computational aerodynamics. *NASA TM-88372 Report*, 1986.
11. Dougherty FC, Benek JA, Steger JL. On applications of chimera grid schemes to store separation. *NASA TM-88193 Report*, 1985.
12. Dougherty FC, Kuan JH. Transonic store separation using a 3-dimensional chimera grid scheme. *AIAA Paper 89-0637*, 1989.
13. Kuan JH, Shih LL, Hu CL. Transonic/viscous turbomachinery flow simulation using a 3-D chimera grid scheme technique. *The 34th National Conference of the Chinese Society of Aeronautics and Astronautics*, vol. 1. Taiwan, 1992; 69–76.
14. Pulliam TH. Euler and thin layer Navier–Stokes codes: ARC2D, ARC3D, *Computational Fluid Dynamics User's Workshop*, vol. 1. The University of Tennessee Space Institute, 1984; 15.1–15.85.
15. Baldwin BS, Lomax H. Thin layer approximation and algebraic model for separated turbulent flows. *AIAA Paper 78-257*, 1978.

